




Flexoelectronic doping of degenerate silicon and correlated electron behaviorPaul C. Lou,^{1,*} Anand Kataiiliha ^{1,*} Ravindra G. Bhardwaj ^{1,*} W. P. Beyermann,²
Dheeraj Mohata,³ and Sandeep Kumar ^{1,†}¹*Department of Mechanical Engineering, University of California, Riverside, California 92521, USA*²*Department of Physics and Astronomy, University of California, Riverside, California 92521, USA*³*Global Communication Semiconductors LLC, Torrance, California 90505, USA*

(Received 2 March 2022; revised 16 May 2022; accepted 19 May 2022; published 10 June 2022)

In the metal/degenerately doped silicon bilayer structure, the interfacial flexoelectric effect due to strain gradient leads to charge carrier transfer from metal layer to the silicon layer. This excess charge carrier concentration is called flexoelectronic doping or flexoelectronic charge transfer, which gives rise to an electronically polarized (order of magnitude larger than ferroelectric materials) silicon layer. In the transport measurements, the charge carrier concentration in silicon is found to increase by two orders of magnitude due to flexoelectronic doping, which changes the Fermi level and the Hall response. The flexoelectronic charge accumulation modifies the electron-electron and the electron-phonon coupling, which gives rise to Mott metal-insulator transition and magnetism of phonons, respectively. The coexistence of flexoelectronic polarization and magnetism gives rise to a class of materials called electronic multiferroics or magnetoelectronics. By controlling the flexoelectronic doping, material behavior can potentially be engineered for quantum, spintronics, and electronics applications in semiconductor materials.

DOI: [10.1103/PhysRevB.105.245112](https://doi.org/10.1103/PhysRevB.105.245112)**I. INTRODUCTION**

Si is a pre-eminent semiconductor that has led to the modern electronics revolution. The ability to dope Si with impurity atoms has allowed control of its conductivity from intrinsic to metal like enabling a multitude of device and circuit applications. Recently, Wang *et al.* [1] demonstrated an alternative method to control interfacial electronic transport using large inner crystal (or bulk) flexoelectric charge separation. The flexoelectric charge separation can also, potentially, be relevant to spintronics, spin caloritronics, and other future applications, and not only electronics. In addition, due to strain, the interfacial flexoelectric polarization [2–4] in thin film heterostructures is expected to be much larger than the bulk counterpart and that too can contribute towards the bulk material response. Hence, the strain gradient can potentially be one of the tools to tailor the properties of a heterostructure for the desired material response.

In a recent study, a large spin-Hall effect was reported in degenerately doped Si under an applied strain gradient, which was an order of magnitude larger than that observed in Pt and similar to the topological insulators surface states [5]. In another study, a large magnetic moment of $1.2 \mu_B/\text{atom}$ due to phonons was reported in the flexoelectronic Si [6]. The measured phonon magnetic moment in highly doped Si was four orders of magnitude larger than that predicted according to the circular motion of ions [7–9]. These responses were attributed to the flexoelectronic polarization in the Si thin

films, but the mechanistic origin of it was not explained. Also, according to the current understanding, no polarization should arise in highly doped semiconductor samples since mobile charge carriers are expected to quench them, which is also supported by the study of Wang *et al.* [1] This contradiction in the observed behavior was attributed to the lack of understanding of the material physics of the underlying bulk and interfacial flexoelectronic behavior in doped semiconductors. This motivated our work since it could give rise to polarization in a conducting material, which could open further opportunities for fundamental and applied materials research.

II. HYPOTHESIS

In semiconductors, strain gradient results in slope in the valence band maxima, the conduction band minima, and the charge carrier mobilities in addition to the band gap. In the case of the lightly doped Si, the slope of the band structure typically results in charge separation and bulk flexoelectric effect as shown in Fig. 1(a) [10]. However, in the case of highly doped Si, the free charge carriers are expected to screen the flexoelectric effect as shown in Fig. 1(a) and thus no net polarization can be detected. In contrast, an interfacial flexoelectric effect [1] appears at the interface in the metal-Si (highly doped) bilayer structure as shown in Fig. 1(b). The interfacial flexoelectric effect [3,11] results in free charge carrier injection from metal layer to the impurity band of the degenerate Si layer as shown in Fig. 1(c). This charge carrier injection is expected to give rise to a gradient of the charge carrier concentration as shown in Fig. 1(d). As a consequence, the flexoelectronic polarization, equal and opposite to the interfacial flexoelectric polarization, is expected to arise in the

*These authors contributed equally to this work.

†Corresponding author: skumar@engr.ucr.edu

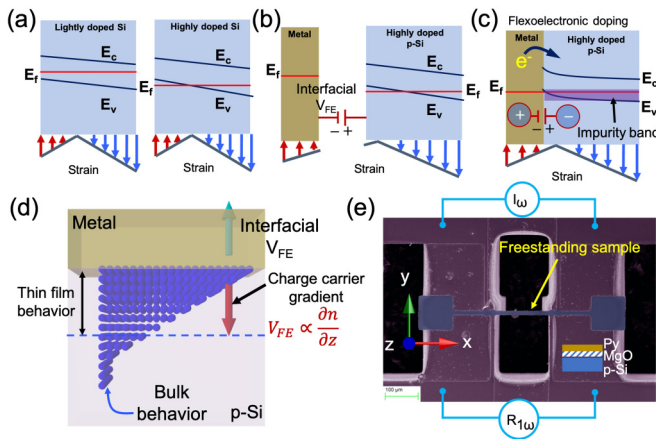


FIG. 1. (a) Schematic showing approximate band diagram of p -doped Si thin film from flexoelectric charge separation due to linearly varying strain (constant strain gradient). (b) Schematic showing the band structure of metal/ p -Si bilayer structure with interfacial flexoelectric voltage due to linearly varying strain (constant strain gradient). (c) Schematic showing the charge carrier injection and flexoelectronic doping in the Py/Si bilayer (cross section) thin film. (d) A schematic showing the charge carrier concentration gradient in the cross-section of the p -Si layer with flexoelectronic polarization equal and opposite to the interfacial flexoelectric polarization. (e) A false color scanning electron micrograph showing the experimental scheme and top view of the device structure with free-standing sample.

bulk of the Si thin film as shown in Figs. 1(c) and 1(d). This effect can be considered an inverse of the behavior reported by Wang *et al.* [1] since the interfacial effect drives the bulk response. In thick Si samples, the flexoelectronic charge carrier gradient is expected to be nearer the interface only as shown in Fig. 1(d). In the case of lightly doped thick Si samples, the behavior will converge with the response reported by Wang *et al.* [1], since there is no impurity band for flexoelectronic doping. Whereas in the thin film (micro/nano) doped Si samples, the average charge carrier density in the highly doped Si layer will increase, for example, from say $5 \times 10^{19} \text{ cm}^{-3}$ to $7 \times 10^{19} \text{ cm}^{-3}$ in addition to the charge carrier concentration gradient as shown in Fig. 1(d). We call this phenomenon flexoelectronic doping of the Si thin films or flexoelectronic charge transfer that is driven by the free electronic charge carriers transferred from metal to Si.

Since Si is no longer charge neutral, flexoelectronic doping is expected to lead to renormalization of the electronic wave function as well as phonons, which would modify the electron-electron and electron-phonon coupling. Hence, both weakly and strongly correlated electronic behavior could potentially be induced in Si thin films. In this study, we report experimental evidence of the large flexoelectronic doping of the degenerate Si layer in the metal-Si heterostructures. This flexoelectronic doping results in about two orders increase in charge carrier concentration from $8.73 \times 10^{18} \text{ cm}^{-3}$ to $1.55 \times 10^{21} \text{ cm}^{-3}$. This charge accumulation further gives rise to strong electron-electron Coulomb repulsion, which results in a Mott metal insulator transition (MIT) in the Si layer. Additionally, the superposition of the flexoelectronic

polarization and phonons gives rise to a magnetic moment in the Si layer and giant magnetoresistance (GMR) response in the sample. As a consequence, metal/Si heterostructures can be considered electronic multiferroic materials.

III. EXPERIMENTAL RESULTS AND DISCUSSION

To study the flexoelectronic doping in Si thin films, we chemically etched a $2\text{-}\mu\text{m}$ single crystal p -Si (Boron doped) device layer ($0.001\text{--}0.005 \Omega \text{ cm}$) of the SOI wafer to achieve the thickness closer to $\sim 400 \text{ nm}$ by successively oxidizing (SiO_2 formation using thermal oxidation) and then etching the thermal oxide using hydrofluoric (HF) acid [12]. This method is designed such that larger strain gradient effects are achieved in Si. The device structure and the backside Si underneath the sample is etched using deep reactive ion etching (DRIE). Then, the MgO (1.8 nm) and $\text{Ni}_{80}\text{Fe}_{20}$ (Py) (25 nm) layers were deposited using sputtering and e -beam evaporation, respectively, on the etched free-standing p -Si thin films structure as shown in Fig. 1(e). The metal and oxide depositions are expected to induce large strain gradient in the Si layer as well as at the interface due to thermal mismatch stresses. Using a qualitatively similar technique, photonics in inhomogeneously strained Si have already been demonstrated [13,14]. Previously, a strain of 4% was estimated using high resolution transmission electron microscope (HRTEM) in $2\text{-}\mu\text{m}$ p -Si near the MgO interface [5]. However, HRTEM sample fabrication can also induce additional strain. Hence, the strain distribution and strain gradient were not measured in this study. The MgO layer is used to prevent any metal diffusion into Si. Based on previous results, the MgO layer was not necessary and was introduced to remove the potential alloying effects at the interface [15,16]. However, the flexoelectric polarization of the MgO layer also contributes towards flexoelectronic doping. The interface quality and sample structure is expected to be similar to previous study [5].

A. Flexoelectronic doping in Py/MgO/ p -Si (400 nm) sample

In the first study, we measured the longitudinal resistance as a function of temperature from 350 to 5 K and current bias from $10 \mu\text{A}$ to 2 mA as shown in Fig. 2(a) inside a Quantum Design PPMS chamber using standard lock-in technique. The sample (sample 1) dimensions are length $160 \mu\text{m}$, width $11.7 \mu\text{m}$, and thickness 400 nm . These responses are significantly different from the Py and p -Si responses, individually [12]. The resistance of the sample reduces as the current bias is increased to 2 mA as shown in Fig. 2(a). The mechanism of the reduction is attributed to the increased strain gradient due to thermal mismatch stresses from self-heating of the free-standing sample [5]. It is noted that Joule heating due to larger current will lead to an increase in resistance as opposed to the observed response, which eliminated Joule heating as the probable cause of the observed behavior. The resistance responses exhibit an MIT below 100 K as shown in Figs. 2(a) and 2(b). The residual resistance after MIT is larger at higher currents as shown in Fig. 2(b). The MIT response cannot arise in the Py layer having metallic bonding. Hence, the Si layer is expected to become an insulator at reduced temperatures. As

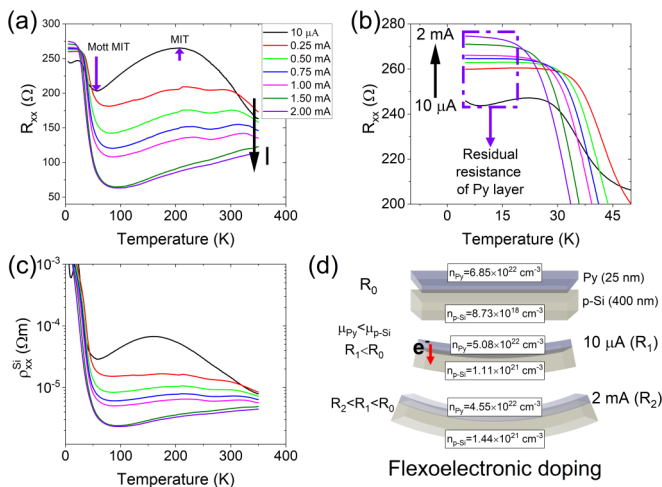


FIG. 2. (a) Longitudinal resistance response in Py (25 nm)/MgO/*p*-Si (400 nm) composite sample as a function of temperature and current bias from 10 μ A to 2 mA, (b) the resistance response between 50 and 5 K showing the Mott metal insulator transition in the Si layer and residual resistance of Py layer, (c) the estimated resistivity of the Si layer in the composite sample after subtracting Py response, and (d) a schematic showing the change in the average charge carrier concentration from flexoelectronic doping of the Si layer due to charge carrier transfer from Py layer to Si layer.

as a consequence, the residual resistance at 5 K is expected to be from the Py layer only, as shown in Fig. 2(b).

The Py resistance response as a function of temperature from 300 to 5 K has been reported previously [12]. From previous data, the resistance of the Py layer in the current sample is expected to be $\sim 182.6 \Omega$ at 5 K as shown in Supplemental Material Fig. S1 [17], whereas the residual resistance is $\sim 245.8 \Omega$ at 10 μ A. The ratio of the measured and expected resistance at 5 K is calculated and used as a multiplication factor to estimate the Py resistance behavior for measurement at each current. We then subtracted the Py resistance response from the sample resistance and extracted the resistivity behavior of the Si layer, which is shown in Fig. 2(c). The estimated resistivity of the *p*-Si layer is an order of magnitude larger than the wafer device layer resistivity, which is a clear indicator of flexoelectronic doping. The resistance in Py/MgO/*p*-Si (400 nm) sample is even smaller than that in the Py/MgO/*p*-Si (2 μ m) sample [18].

The flexoelectronic doping is attributed to charge carrier transfer from the Py to the *p*-Si layer. We divided $n_{py} = 6.85 \times 10^{22} \text{ cm}^{-3}$ with the multiplication factor (calculated earlier) to estimate the new charge carrier concentration as well as the change in the charge carrier concentration for each current dependent measurement presented in Fig. 2(a). For example, the difference in charge carrier concentration is expected to be $1.96 \times 10^{22} \text{ cm}^{-3}$ at 10 μ A of current in the Py layer. The difference in the charge carrier concentration is then transferred to the Si layer. As a result, the new charge carrier concentration of Si at 10 μ A of current increases to $1.11 \times 10^{21} \text{ cm}^{-3}$ as shown in Fig. 2 (d) as compared to $\sim 8.73 \times 10^{18} \text{ cm}^{-3}$ measured from the *p*-Si (400 nm) sample as shown in Supplemental Material Fig. S2 [17]. The

flexoelectronic doping value is similar to one of the highest doping levels achieved in Si [19] using impurities. The increased sample bending from larger current bias results in larger flexoelectronic doping as shown in Fig. 2(d) and the Supplemental Material. The mobility of the charge carrier in *p*-Si ($\sim 131.4 \text{ cm}^2/\text{V s}$) is two orders of magnitude larger than that in Py ($\sim 1.7 \text{ cm}^2/\text{V s}$) as shown in Supplemental Material Fig. S2, which is the underlying cause of the reduction in the overall resistance due to flexoelectronic doping. The charge carrier concentration estimated in this study is an average value and a gradient of charge carrier is expected to exist due to the gradient in the band structure as stated earlier. Using the resistivity and charge carrier concentration data, we calculated the change in mobility of the flexoelectronic Si layer. The mobility at 10 μ A and 300 K is expected to be $3.88 \text{ cm}^2/\text{V s}$, which then increases to $10.61 \text{ cm}^2/\text{V s}$ at 2 mA as shown in Supplemental Material Table S1 [17]. These values are significantly smaller than the Hall mobility ($\sim 131.4 \text{ cm}^2/\text{V s}$) measured for the *p*-Si only sample as shown in Supplemental Material Fig. S2. This behavior is attributed to the charging effect from the excess charge carrier and, possibly, electron-electron Coulomb repulsion. It is noted that strain gradient accompanied the gradient of mobilities through the thickness of the sample. However, its effect on charge transport and flexoelectronic doping is not characterized.

The change in charge carrier concentration is calculated for each current as shown in Supplemental Material Table S1. Based on the number of charge carrier injected, we estimated the maximum charge accumulation in Si layer to be $71.1 \text{ C}/\text{m}^2$ at 10 μ A of current, which is three orders of magnitude larger than the value reported recently by Wang *et al.* [1] and is expected to increase to $79.4 \text{ C}/\text{m}^2$ at 2 mA due to the larger strain gradient. This value is also an order of magnitude larger than the ferroelectric polarization ($1.5 \text{ C}/\text{m}^2$) [20] even though a direct comparison is not possible due to the electronic nature of the charge accumulation in this study. The phonon magnetic moment from dynamical multiferroicity arises from the circular ionic motion from optical phonons [7]. As a consequence, the predicted value of the phonon magnetic moment is expected to be $10^{-4} \mu_B$ [7]. However, the flexoelectronic doping arises due to a large increase in free electronic charge carriers, which is expected to give rise to a large Born effective charge. Hence, this large charge carrier accumulation is believed to be the underlying cause of the phonon magnetic moment of $1.2 \mu_B/\text{atom}$ in flexoelectronically doped Si [6] as compared to $10^{-4} \mu_B$ [7] predicted by the dynamical multiferroicity. The charge accumulation also shows that the flexoelectric effect at interfaces can be very large and should not be ignored.

Our resistance measurements showed an MIT behavior below 100 K, as stated earlier. Another MIT-like behavior is observed at 200 K, but only in the measurement at 10 μ A current bias. In B-doped Si, the MIT occurred as a function of the doping at $\sim 3\text{--}4 \times 10^{18} \text{ cm}^{-3}$ [21,22]. However, in the present study, the *p*-Si layer is already degenerately doped ($\sim 8.73 \times 10^{18} \text{ cm}^{-3}$) as shown in Supplemental Material Figure S2. Hence, flexoelectronic charge accumulation is expected to be the underlying cause of MIT behavior. The excess charge carriers from flexoelectronic doping are

expected to modify the electron-electron Coulomb repulsion and possibly open a gap, which led to Mott transition [21,23] below 100 K as shown in Figs. 2(a)–2(c). The electron-electron Coulomb repulsion is expected to be weaker at higher temperatures due to thermal relaxation. The weaker Coulomb repulsion drove a continuous MIT at 200 K for an applied 10- μ A current, as shown in Fig. 2(a). In the case of higher current, the self-heating will increase the thermal relaxation and suppress the electron-electron Coulomb repulsion, which is supported by the gradual change in the resistance behavior as a function of temperature (negative temperature coefficient of resistance) in measurements at higher currents as shown in Fig. 2(a). In measurements at 1.5 and 2 mA, the electron-electron Coulomb repulsion is completely suppressed, potentially, due to thermal relaxation. The MIT response is not observed in Py/MgO/*p*-Si (2 μ m) samples due to a smaller strain gradient and consequently smaller flexoelectronic doping [18]. At this time, the band structure of the flexoelectronically doped Si is not available, which is part of the future theoretical work. The observed Mott MIT is an example of correlated electronic behavior due to the change in electron-electron interactions from flexoelectronic doping. It is noted that the flexoelectronic doping level is similar to the doping level achieved in superconducting Si [19]. However, the charge polarization from flexoelectronic doping results in a Mott MIT at much higher temperature instead of superconductivity at $T_c = 0.35$ K [19]. While we did not study superconductivity in our samples, further research may make it feasible.

B. Flexoelectronic spin current in Py/MgO/*p*-Si (400 nm) sample

In the absence of an external magnetic field, the charge carrier injection from the ferromagnetic (Py) layer to the *p*-Si layer is not spin polarized and only an equilibrium charge carrier injection (j_c) is expected to exist. However, an applied magnetic field results in spin polarization of the charge carriers in the ferromagnetic layer. As a consequence, charge carrier injection will be accompanied by a flexoelectronic spin current (j_s) as shown in Fig. 3(a). To study it, we measured the longitudinal resistance as a function of temperature for an applied out-of-plane magnetic field of 0 and 1 T at a current bias of 1 mA in sample 1 as shown in Fig. 3(a). The longitudinal resistance is $\sim 54.5\%$ smaller at ~ 85 K in the case of applied magnetic field as compared to zero field as shown in Fig. 3(a). This reduction in resistance is attributed to reduced scattering due to larger ferromagnetic exchange interactions and reduced Coulomb repulsion from enhanced spin polarization in the Si layer. The reduction in resistance can also be attributed to spin-to-charge conversion from flexoelectronic spin current. The Mott-MIT response as well as residual resistance are similar. The large flexoelectronic spin current is also potentially the reason for the large spin-Hall effect as well as the spin-Seebeck effect reported in Si thin films [5,16,24].

C. Hall effect measurement in Py/MgO/*p*-Si samples

The transfer of the large number of charge carriers from the Py layer to the *p*-Si layer is expected to change the Fermi

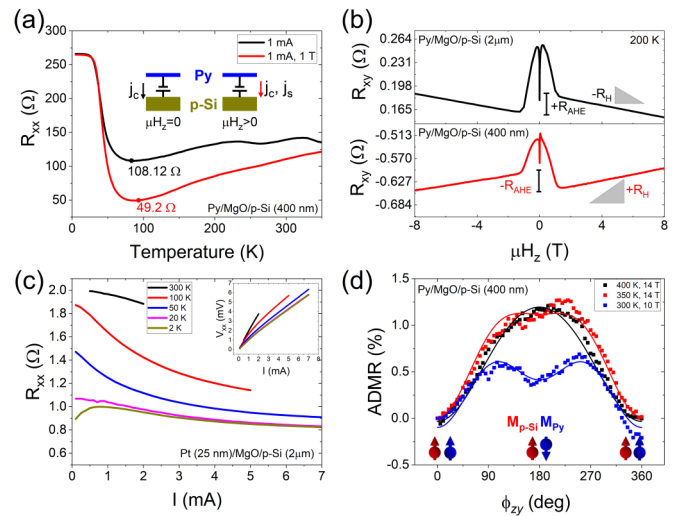


FIG. 3. (a) Longitudinal resistance response in Py (25 nm)/MgO/*p*-Si (400 nm) composite sample at an applied current bias of 1 mA for a zero applied magnetic field and 1 T out of plane magnetic field. (b) The Hall resistance measurement for an applied magnetic field of 8 to -8 T at 200 K showing negative Hall resistance in Py (25 nm)/MgO (1.8 nm)/*p*-Si (2 μ m) in top panel and positive Hall resistance in Py (25 nm)/MgO (1.8 nm)/*p*-Si (400 nm) in bottom panel. (c) The resistance as a function of current measured at 300, 100, 50, 20, and 2 K in a Pt (25 nm)/MgO (1.8 nm)/*p*-Si (2 μ m) sample. Inset shows voltage vs the current response. (d) The angle dependent magnetoresistance measured in free-standing Py/MgO/*p*-Si (400 nm) sample showing the GMR response, which decreases with temperature. The solid line shows the curve fit.

level and, as a consequence, Hall resistance behavior. We then measured the Hall resistance as a function of magnetic field from 8 to -8 T at 200 K in Py(25 nm)/MgO(1.8 nm)/*p*-Si (400 nm) (sample 2) and compared it with a Py(25 nm)/MgO(1.8 nm)/*p*-Si (2 μ m) (sample 3). The sample dimensions are length 40 μ m and width 14 μ m. In the 2- μ m *p*-Si sample, the Hall resistance is negative corresponding to electrons and the anomalous Hall resistance is positive as shown in top panel in Fig. 3(b), whereas in the 400-nm *p*-Si sample, the sign of both the Hall resistance and the anomalous Hall resistance are reversed as shown in the bottom panel in Fig. 3(b). The positive Hall resistance corresponded to holes, which is expected to arise due to the flexoelectronic charge carrier transfer from Py to *p*-Si. Similarly, the anomalous Hall response in Py is due to an intrinsic mechanism [25]. As a consequence, its sign reversal also corresponds to the change in the type of the charge carrier from electrons to holes. A similar electron to hole transition was previously reported in a Pt/MgO/*p*-Si sample [6]. Since the MgO and Py layer thicknesses are the same in both samples, the strain gradient is expected to be smaller in the 2- μ m *p*-Si sample as compared to the 400-nm *p*-Si sample because the critical stress required for beam buckling will be larger in the thicker sample. As a consequence, the smaller flexoelectronic charge carrier transfer will not change the sign of Hall resistance in the case of 2- μ m *p*-Si in sample 3 as opposed to the larger strain gradient and flexoelectronic doping in case of the 400-nm *p*-Si layer in sample 2. This measurement provides a second proof of flexoelectronic dop-

ing. In addition, it shows that the electronic properties can potentially be controlled using a strain gradient even in the case of metal and degenerately doped Si heterostructures.

D. Flexoelectronic doping in Pt/MgO/*p*-Si (2 μ m) sample

For additional experimental proof of the flexoelectronic doping, we fabricated a Pt (25 nm)/MgO (1.8 nm)/*p*-Si (2 μ m) thin film Hall bar sample (sample 4), which allowed us to uncover the effect of electronic source metal layers. The sample dimensions are length 40 μ m and width 14 μ m. We measured the resistance as a function of applied longitudinal current and temperature as shown in Fig. 3(c). The resistivity of the Pt thin film is expected to be $2.57 \times 10^{-7} \Omega \text{ m}$ [6] whereas the resistivity of the Si device layer is expected to be $1\text{--}5 \times 10^{-5} \Omega \text{ m}$. However, the resistance of the sample at 300 K is measured to be 2.02 Ω as compared to 9.61 Ω (using the smallest resistivity of the *p*-Si layer). The measured resistance could not be lower than 6.35 Ω even if we use the bulk resistivity value for Pt ($1 \times 10^{-7} \Omega \text{ m}$). The new resistivity of the Si layer needed to simulate the observed sample resistance is estimated to be $1.518 \times 10^{-6} \Omega \text{ m}$, which could only occur due to charge carrier transfer from the Pt layer to the Si layer due to the strain gradient. This value of the resistivity is smaller than the estimated value in the *p*-Si (400 nm) sample as shown in Fig. 2(c). The melting point of Pt is significantly higher than Py and, as a consequence, the residual stresses in the Pt layer are expected to be larger, which is expected to be the underlying cause of larger flexoelectronic charge transfer and doping. This reduction in resistance due to flexoelectronic charge carrier transfer is attributed to the larger mobility of charge carriers in *p*-Si as compared to metal, as stated earlier. The larger current should increase the resistance of the sample due to self-heating since both Pt and *p*-Si have positive temperature coefficient of resistance (TCR) individually [26]. However, the resistance of the sample decreases as shown in Fig. 3(c), which is expected to arise due to flexoelectronic charge carrier transfer. This behavior is similar to the previously reported spin-Hall magnetoresistance response as a function of current [5]. The self-heating effect cannot be eliminated by controlling the experimental chamber temperature because the change in chamber temperature is uniform whereas the self-heating is restricted to the free-standing sample only. The voltage drop as a function of current also shows a nonlinear behavior as shown in the inset of Fig. 3(c). This behavior is again attributed to the larger strain gradient from self-heating and larger flexoelectronic doping of the Si layer. This is the third experimental evidence of flexoelectronic doping of Si layer in a metal/Si bilayer structure. In the Py/*p*-Si (400 nm) sample, the charge carrier injection also led to exchange interactions, which led to Mott MIT. However, we do not observe Mott MIT in the Pt/*p*-Si (2 μ m) sample even though the flexoelectronic doping levels are expected to be larger. We attribute this behavior to the absence of ferromagnetic proximity-induced exchange interactions. This measurement showed that by controlling the kind of flexoelectronic doping, the correlated electron behavior can potentially be controlled. We also propose that flexoelectronic doping from different metals (lighter or heavier) will lead to

different correlated electron behavior, which is part of the future work.

E. Giant magnetoresistance response in Py/MgO/*p*-Si (400 nm) sample

The superposition of flexoelectronic polarization and temporal polarization of phonons gives rise to temporal magnetic moment due to dynamical multiferroicity, as reported previously. The dynamical multiferroicity in Si thin films under an applied strain gradient [6] can be described as

$$\mathbf{M}_t \propto \mathbf{P}_{\text{FE}} \times \partial_t \mathbf{P} \quad (1)$$

where \mathbf{M}_t , $\partial_t \mathbf{P}$, and \mathbf{P}_{FE} ($\propto \frac{\partial n}{\partial z}$) are the temporal magnetic moment, time-dependent polarization of optical phonons, and flexoelectronic effect [1] from charge carrier concentration gradient, respectively. To measure the magnetism, we measured the angle-dependent magnetoresistance of the sample as a function of temperature in sample 1 as shown in Fig. 3(d). The angle-dependent magnetoresistance in the *zy* plane (plane perpendicular to current direction) at 400 K and 14 T showed a $\cos \theta_{zy}$ angular symmetry, which is attributed to the GMR for a current in-plane (CIP) geometry. The GMR is $\sim 1.22\%$ at 14 T magnetic field as shown in Fig. 3(d). Based on symmetry, the magnetic moment in the Si layer is expected to be in the $+z$ direction and remained fixed, while the Py magnetic moment always aligned with the magnetic field giving rise to the GMR response as shown in Fig. 3(d). The response at 350 K is similar, but the magnitude of the GMR reduces to 1.11% at 14 T magnetic field as shown in Fig. 3(d). At 300 K, the GMR response decreases to $\sim 0.51\%$ at 10 T magnetic field. The additional $\sin^2 \theta_{zy}$ response at 350 and 300 K is attributed to anisotropic magnetoresistance (AMR) from the Py layer. The reduction in the GMR response as a function of temperature is attributed to the magnetism of phonons or dynamical multiferroicity. The reduction in temperature causes the reduction in polarization of the optical phonons, which in turn reduces the temporal magnetic moment. The observed magnetic behavior is a second example of correlated electron behavior due to modification in electron-phonon coupling [27] from flexoelectronic doping. In addition, the coexistence of flexoelectronic polarization and magnetism is attributed to dynamical multiferroicity. As a consequence, the metal/Si (doped) heterostructures can be called magnetoelectronic multiferroic, which is a different class of materials.

While we have demonstrated flexoelectronic doping and resulting magnetism and Mott MIT, the quantitative relationship with the strain gradient is not measured. Currently, there is no known method to address it since the samples are conducting. Additionally, the flexoelectronic charge transfer creates a charge deficient metal layer, which could give rise to correlated electron behavior in metal layers as well. The flexoelectronic behavior in the metal layer can have a potential application in catalysis. The future theoretical studies are also needed to uncover the changes in the band structure, renormalization of the electronic wave function, and phonons, which is a modeling challenge due to lack of charge neutrality in the flexoelectronic doping.

IV. CONCLUSION

In conclusion, we present experimental evidence of large flexoelectronic doping in a degenerately B-doped Si. The flexoelectronic doping arises from the charge carrier injection from the metal layer to the Si layer due to interfacial flexoelectric effect. The flexoelectronic doping gives rise to electron-electron Coulomb repulsion and Mott MIT. Additionally, flexoelectronic doping gives rise to magnetic moment in Si due to electronic dynamical multiferroicity. The discovery of flexoelectronic doping in semiconductors has opened a different direction in materials research, which

can be applied to quantum, spintronics, and electronics device applications.

ACKNOWLEDGMENTS

The fabrication of experimental devices was completed at the Center for Nanoscale Science and Engineering at UC Riverside. Electron microscopy imaging was performed at the Central Facility for Advanced Microscopy and Microanalysis at UC Riverside. S.K. acknowledges a research gift from Dr. S. Kumar.

-
- [1] L. Wang, S. Liu, X. Feng, C. Zhang, L. Zhu, J. Zhai, Y. Qin, and Z. L. Wang, *Nat. Nanotechnol.* **15**, 661 (2020).
 - [2] T. D. Nguyen, M. Sheng, Y. Yao-Wen, P. K. Purohit, and M. C. McAlpine, *Adv. Mater.* **25**, 946 (2013).
 - [3] D. Lee and T. W. Noh, *Philos. Trans. R. Soc., A* **370**, 4944 (2012).
 - [4] S. Das, B. Wang, T. R. Paudel, S. M. Park, E. Y. Tsymbal, L.-Q. Chen, D. Lee, and T. W. Noh, *Nat. Commun.* **10**, 537 (2019).
 - [5] P. C. Lou, A. Katailaha, R. G. Bhardwaj, T. Bhowmick, W. P. Beyermann, R. K. Lake, and S. Kumar, *Phys. Rev. B* **101**, 094435 (2020).
 - [6] P. C. Lou, A. Katailaha, R. G. Bhardwaj, W. P. Beyermann, D. M. Juraschek, and S. Kumar, *Nano Lett.* **21**, 2939 (2021).
 - [7] D. M. Juraschek, M. Fechner, A. V. Balatsky, and N. A. Spaldin, *Phys. Rev. Materials* **1**, 014401 (2017).
 - [8] K. Dunnett, J. X. Zhu, N. A. Spaldin, V. Juričić, and A. V. Balatsky, *Phys. Rev. Lett.* **122**, 057208 (2019).
 - [9] D. M. Juraschek and N. A. Spaldin, *Phys. Rev. Materials* **3**, 064405 (2019).
 - [10] D.-B. Zhang and K. Chang, *arXiv:2008.11452*.
 - [11] D. Tian, Y. Hou, Q. Pan, and B. Chu, *Phys. Rev. Applied* **14**, 034008 (2020).
 - [12] P. C. Lou and S. Kumar, *Phys. Status Solidi B* **255**, 1700545 (2018).
 - [13] C. Schrieffer, F. Bianco, M. Cazzanelli, M. Ghulinyan, C. Eisenschmidt, J. de Boor, A. Schmid, J. Heitmann, L. Pavesi, and J. Schilling, *Adv. Opt. Mater.* **3**, 129 (2015).
 - [14] M. Cazzanelli, F. Bianco, E. Borga, G. Pucker, M. Ghulinyan, E. Degoli, E. Luppi, V. Vénier, S. Ossicini, D. Modotto, S. Wabnitz, R. Pierobon, and L. Pavesi, *Nat. Mater.* **11**, 148 (2011).
 - [15] P. C. Lou and S. Kumar, *Solid State Commun.* **259**, 24 (2017).
 - [16] R. G. Bhardwaj, P. C. Lou, and S. Kumar, *Appl. Phys. Lett.* **112**, 042404 (2018).
 - [17] See Supplemental Material at <http://link.aps.org/supplemental/10.1103/PhysRevB.105.245112> for flexoelectronic charge transfer calculations, Py resistance measurement, and p-Si Hall effect measurement data.
 - [18] P. C. Lou, W. P. Beyermann, and S. Kumar, *J. Appl. Phys.* **122**, 123905 (2017).
 - [19] E. Bustarret, C. Marcenat, P. Achatz, J. Kačmarčík, F. Lévy, A. Huxley, L. Ortéga, E. Bourgeois, X. Blase, D. Débarre, and J. Boulmer, *Nature (London)* **444**, 465 (2006).
 - [20] K. Y. Yun, D. Ricinschi, T. Kanashima, M. Noda, and M. Okuyama, *Jpn. J. Appl. Phys.* **43**, L647 (2004).
 - [21] N. Mott, *Adv. Phys.* **21**, 785 (1972).
 - [22] N. F. Mott and M. Kaveh, *Philos. Mag. B* **47**, 577 (1983).
 - [23] N. Mott, *J. Solid State Chem.* **88**, 5 (1990).
 - [24] R. G. Bhardwaj, P. C. Lou, and S. Kumar, *Phys. Status Solidi RRL* **12**, 1800064 (2018).
 - [25] N. Nagaosa, J. Sinova, S. Onoda, A. H. MacDonald, and N. P. Ong, *Rev. Mod. Phys.* **82**, 1539 (2010).
 - [26] P. C. Lou and S. Kumar, *J. Phys.: Condens. Matter* **30**, 145801 (2018).
 - [27] B. Cheng, T. Schumann, Y. Wang, X. Zhang, D. Barbalas, S. Stemmer, and N. P. Armitage, *Nano Lett.* **20**, 5991 (2020).